© 2015. Published by The Company of Biologists Ltd | Development (2015) 142, 672-680 doi:10.1242/dev.120279

RESEARCH ARTICLE

Vascular patterning regulates interdigital cell death by a ROS-mediated mechanism

Idit Eshkar-Oren[1,*], Sharon Krief[1,*], Napoleone Ferrara[2], Alison M. Elliott[3] and Elazar Zelzer[1,‡]

ABSTRACT

Blood vessels serve as key regulators of organogenesis by providing oxygen, nutrients and molecular signals. During limb development, programmed cell death (PCD) contributes to separation of the digits. Interestingly, prior to the onset of PCD, the autopod vasculature undergoes extensive patterning that results in high interdigital vascularity. Here, we show that in mice, the limb vasculature positively regulates interdigital PCD. *In vivo*, reduction in interdigital vessel number inhibited PCD, resulting in syndactyly, whereas an increment in vessel number and distribution resulted in elevation and expansion of PCD. Production of reactive oxygen species (ROS), toxic compounds that have been implicated in PCD, also depended on interdigital vascular patterning. Finally, *ex vivo* incubation of limbs in gradually decreasing oxygen levels led to a correlated reduction in both ROS production and interdigital PCD. The results support a role for oxygen in these processes and provide a mechanistic explanation for the counterintuitive positive role of the vasculature in PCD. In conclusion, we suggest a new role for vascular patterning during limb development in regulating interdigital PCD by ROS production. More broadly, we propose a double safety mechanism that restricts PCD to interdigital areas, as the genetic program of PCD provides the first layer and vascular patterning serves as the second.

KEY WORDS: Programmed cell death, Vascular patterning, Reactive oxygen species, Interdigit, Oxygen, Limb development, Syndactyly

INTRODUCTION

In the mouse embryo, the limbs emerge at embryonic day (E) 9.5, consisting of a mesenchymal core covered by ectoderm. The distal tip of the ectoderm forms a specialized epithelial structure known as the apical ectodermal ridge (AER), which acts as a major signaling center for limb patterning. Soon afterwards, mesenchymal cells form precartilaginous condensations that will serve as templates for the various skeletal elements, including the digits (Cooper et al., 2011; Johnson and Tabin, 1997; Zeller et al., 2009).

The developing digits are initially connected by soft tissue. During limb morphogenesis, the digits are separated by coordinated regression of the soft tissue through programmed cell death (PCD) and outgrowth of the digits (Fallon and Cameron, 1977; Fernandez-Teran et al., 2006; Zuzarte-Luis and Hurle, 2002). Interdigital PCD commences at E12.5 in the mesenchyme underlying the AER. It then spreads proximally and by E14.0 it extends throughout the interdigital spaces, forming well-defined regions of cell death. By E14.5, most of the distal interdigital tissue has regressed and the digits are almost completely separated, as PCD is still active in the remaining proximal interdigital soft tissue (Fernandez-Teran et al., 2006; Salas-Vidal et al., 2001).

Extensive work aimed at exposing the regulatory signals of PCD has concentrated mostly on the AER and interdigital mesenchyme as potential sources of these signals. Fibroblast growth factors (FGFs) produced by the AER were shown to act as negative regulators of PCD (Fernandez-Teran and Ros, 2008; Hernández-Martínez and Covarrubias, 2011; Montero et al., 2001). Bone morphogenetic proteins (BMP) 2, 4 and 7 are expressed in the AER and interdigital mesenchyme prior to the onset of PCD. BMPs were suggested to promote PCD by acting directly on interdigital tissue (Guha et al., 2002; Macias et al., 1997; Zou and Niswander, 1996) or indirectly, by downregulating the expression of FGFs in the AER (Maatouk et al., 2009; Pajni-Underwood et al., 2007). Similarly, the transcription factors MSX1 and MSX2 have been shown to act downstream of the BMP signaling pathway in the regulation of interdigital PCD (Lallemand et al., 2005). Retinoic acid (RA) is another molecule that has been implicated in PCD. RA was shown to affect the interdigital mesenchyme by upregulation of *Bmp* genes in that region (Dupé et al., 1999; Rodriguez-Leon et al., 1999). In the AER, RA was suggested to antagonize the survival effect of FGFs (Hernandez-Martinez et al., 2009).

Reactive oxygen species (ROS) are chemically reactive molecules that are generated through the partial reduction of molecular oxygen (O_2). ROS are produced mostly in the mitochondria, as a byproduct of the respiratory chain. These toxic compounds might damage cells by oxidizing constituents such as DNA, proteins and lipids (Bokov et al., 2004). ROS were shown to participate in the regulation of interdigital PCD in mouse embryos (Covarrubias et al., 2008). During mouse development, high levels of ROS were detected at interdigital regions and coincided with areas of PCD. Treatment with antioxidants caused reduction of PCD and interdigital regression, supporting a role for ROS in the activation of PCD (Salas-Vidal et al., 1998). Moreover, expression patterns of specific antioxidant enzymes determined ROS production and PCD at interdigital areas (Schnabel et al., 2006).

During organ development, blood vessels not only supply oxygen and nutrients but also provide vital regulatory signals (Cleaver and Melton, 2003; Coultas et al., 2005; Nikolova and Lammert, 2003; Tirziu and Simons, 2009). Vascular impairments during embryogenesis can lead to aberrant organ formation and lethality (Carmeliet, 2005; Ferrara et al., 1996; Gao et al., 2005; Lammert et al., 2003; Matsumoto et al., 2001). During the initial stages of mouse limb development, the mesenchyme core is vascularized by a primary unpatterned vascular plexus, which is formed by sprouts from the dorsal aorta and by somite-derived angioblasts that invade the limb bud (Coffin and Poole, 1988; Drake et al., 1998; Folkman, 2003; Risau and Flamme, 1995; Sabin, 1920;

[1]Department of Molecular Genetics, Weizmann Institute of Science, Rehovot 76100, Israel. [2]Genentech, Inc., 1 DNA Way, S. San Francisco, CA 94080, USA. [3]Departments of Pediatrics and Child Health and Biochemistry and Medical Genetics, University of Manitoba, Winnipeg, MB R3A 1S1, Manitoba, Canada.
*These authors contributed equally to this work

‡Author for correspondence (eli.zelzer@weizmann.ac.il)

Received 25 November 2014; Accepted 11 December 2014

Development (2015) 142, 672-680 doi:10.1242/dev.120279

Sato and Loughna, 2002). Between E10.5 and E12.5, the primary vascular plexus undergoes extensive patterning. Blood vessels regress from areas of emerging cartilage anlagen and rearrange into a highly branched and rich network, which is segregated from the condensation areas (Feinberg et al., 1986; Hall and Miyake, 1992; Seichert and Rychter, 1972). Previously, we showed that the condensing mesenchyme serves as a signaling center for the limb vasculature. In our previous study, expression of vascular endothelial growth factor (*Vegf*) by condensing mesenchymal cells was shown to control the rearrangement of the primary vascular plexus into the stereotypical enriched and segregated network that surrounds the developing skeleton (Eshkar-Oren et al., 2009).

Interestingly, one of the consequences of this extensive patterning is vascular enrichment at interdigital zones prior to the onset of PCD. The concept of vascular enrichment of a tissue destined to undergo degradation is counterintuitive. Vascularization is normally associated with development and growth, rather than with tissue regression and cell death (Tirziu and Simons, 2009). Furthermore, hypoxic conditions in the embryo are often associated with abnormal development and cell death (Dunwoodie, 2009). In this work, we revisit the question of the role of vascular patterning in interdigital PCD in a mouse model. We show that reduction in vessel number in interdigital areas inhibits PCD, resulting in syndactyly,

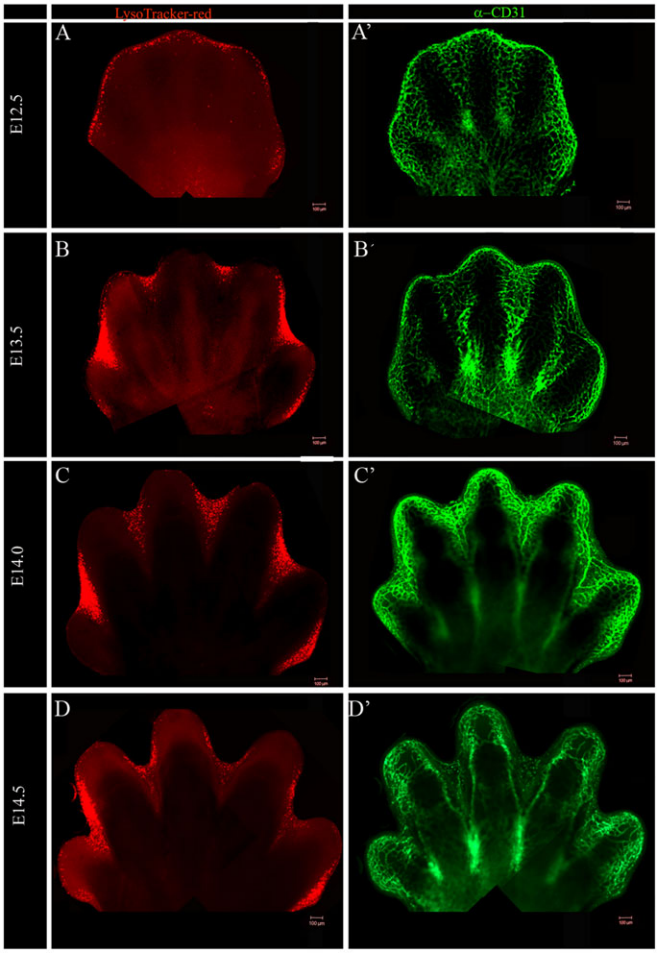

Fig. 1. Interdigital areas are vascularized during PCD. Whole-mount autopods from WT mice immunostained with LysoTracker red for PCD (A-D) and with anti-CD31 antibody (green) for vascular endothelial cells (A′-D′) at E12.5 (A,A′), E13.5 (B,B′), E14 (C,C′) and E14.5 (D,D′). Scale bars: 100 µm.

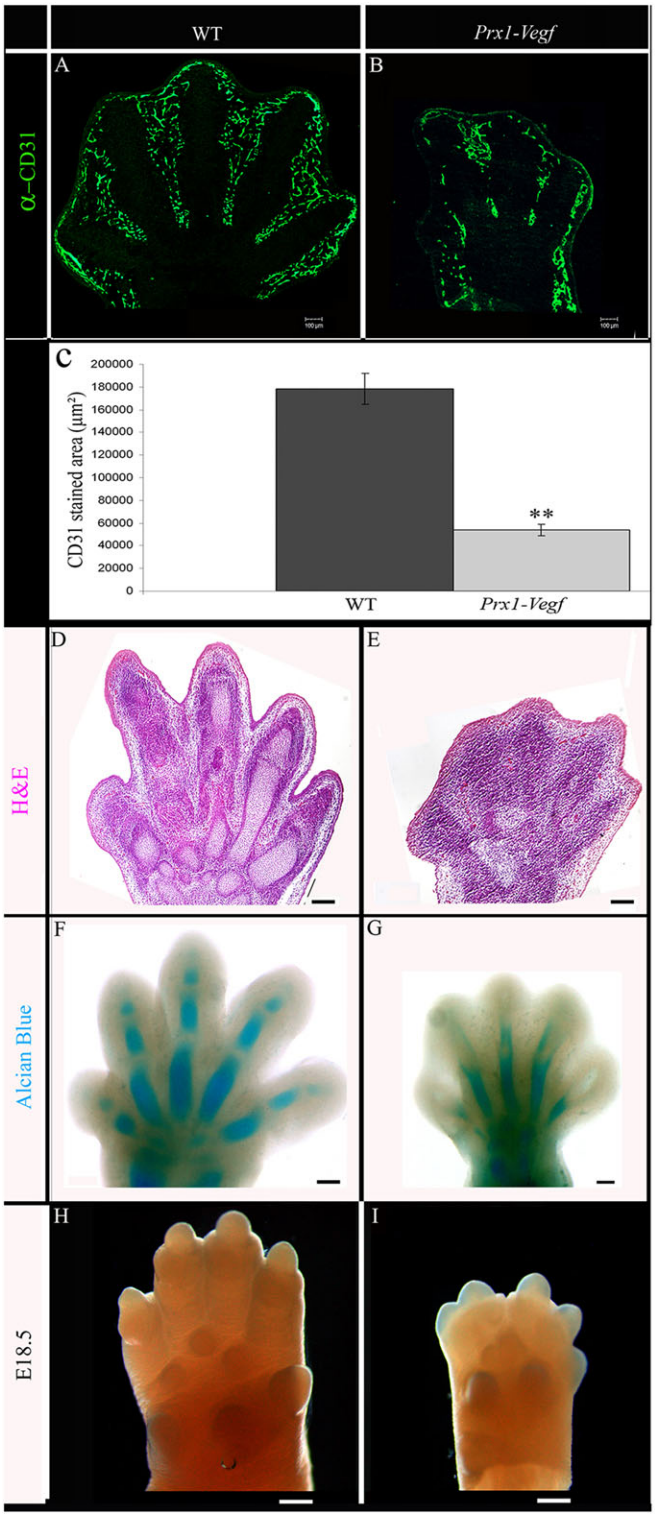

Fig. 2. A decrease in interdigital blood vessels leads to failure of soft tissue regression. (A,B) Cross-sections of E13.5 WT (A) and *Prx1-Vegf* (B) autopods immunostained with anti-CD31 antibody (green) for vascular endothelial cells. (C) Comparison between cross-sections from E13.5 WT and *Prx1-Vegf* embryos reveals a threefold decrease in vessel density in the mutant. n=40 sections from four different limbs; $^{**}P<0.05$; data represented as the mean±s.e.m. (D,E) H&E staining of cross-sections from E14.5 WT (D) and *Prx1-Vegf* (E) autopods. (F,G) Alcian Blue staining of E15.5 WT (F) and *Prx1-Vegf* (G) whole-mount autopods. (H,I) E18.5 autopods of WT (H) and *Prx1-Vegf* (I) embryos. Ellipses indicate digits, arrows indicate interdigital areas. Scale bars: 100 µm in A-G; 1 mm in H,I.

Development (2015) 142, 672-680 doi:10.1242/dev.120279

whereas increased vascularity results in elevated PCD. We then demonstrate the dependency of PCD on oxygen level and show that ROS production depends on interdigital vessel number and oxygen level. Based on these findings, we propose a model for the role of limb vasculature in PCD, whereby a high density of blood vessels in the interdigital zone leads to an elevation in tissue oxygenation, which is needed for ROS production and, as a consequence, for PCD.

RESULTS

Interdigital areas are highly vascularized during PCD

Previously, we demonstrated that the limb vasculature undergoes extensive patterning during the initial stages of skeletogenesis (Eshkar-Oren et al., 2009). To examine the possible role of the vasculature in interdigital PCD, we analyzed vascular patterning during PCD in wild-type (WT) limbs at E12.5-E14.5 (Fig. 1). At E12.5, interdigital PCD initiated mostly in the AER and in the underlying mesenchyme (Fig. 1A). At that stage, a complex and branched high-density capillary network was seen at the interdigital areas, whereas the forming digits were unvascularized (Fig. 1A′). At E13.5, although cell death extended laterally and proximally into the interdigital regions (Fig. 1B), the capillary network was maintained (Fig. 1B′). At E14, extensive interdigital PCD continued (Fig. 1C); concurrently, the interdigital vasculature started to undergo a remodeling process, whereby the highly branched network was replaced with prominent blood vessels (Fig. 1C′). By E14.5, PCD ended and interdigital vascular patterning was completed (Fig. 1D, D′). These results show that vessel regression occurs at advanced stages of interdigital PCD and not at the onset, thus negating the possibility that the former triggers the latter.

A decrease in the number of interdigital blood vessels leads to inhibition of PCD

The notion of vascular enrichment occurring prior to and during interdigital PCD is counterintuitive, because blood vessels are associated with tissue growth. To study this seeming contradiction, we sought to manipulate limb vasculature and analyze the effect on interdigital PCD. To assess the effect of reduced vessel number, we examined limbs in which *Vegf* was inactivated in the mesenchyme using the *Prx1-Cre* mouse as a deleter (Gerber et al., 1999; Logan et al., 2002). Previously, we demonstrated a prominent reduction in limb vessel number in these mice (Eshkar-Oren et al., 2009). Analysis of E13.5 limbs revealed, as expected, a severe reduction in vessel number, in particular at interdigital areas (Fig. 2A-C). Histological sections and Alcian Blue staining of limbs at E14.5-E15.5 (Fig. 2D-G), as well as whole limbs of E18.5 embryos (Fig. 2H,I), revealed that, in the mutant, soft tissue was maintained between the forming digits, suggesting abnormal interdigital PCD.

To study interdigital PCD in autopods with reduced vasculature, we compared LysoTracker (Fig. 3A,B), TUNEL (Fig. 3C,D) and active caspase-3 (Fig. 3E-G) staining of WT and *Prx1-Vegf* embryos at E13.5. In contrast to control limbs, PCD was not detected in the interdigital mesenchymal cells of *Prx1-Vegf* limbs; instead, restricted cell death was observed in chondrocytes of the forming digits, probably as a result of increased hypoxia. The finding that a reduction in interdigital vessel number leads to syndactyly associated with the absence of PCD suggests that interdigital vessels are necessary for PCD.

An alternative interpretation of the results is that vascular reduction during early stages of limb development inhibits interdigital PCD indirectly, by causing general developmental abnormalities. To test this possibility, we analyzed the expression of

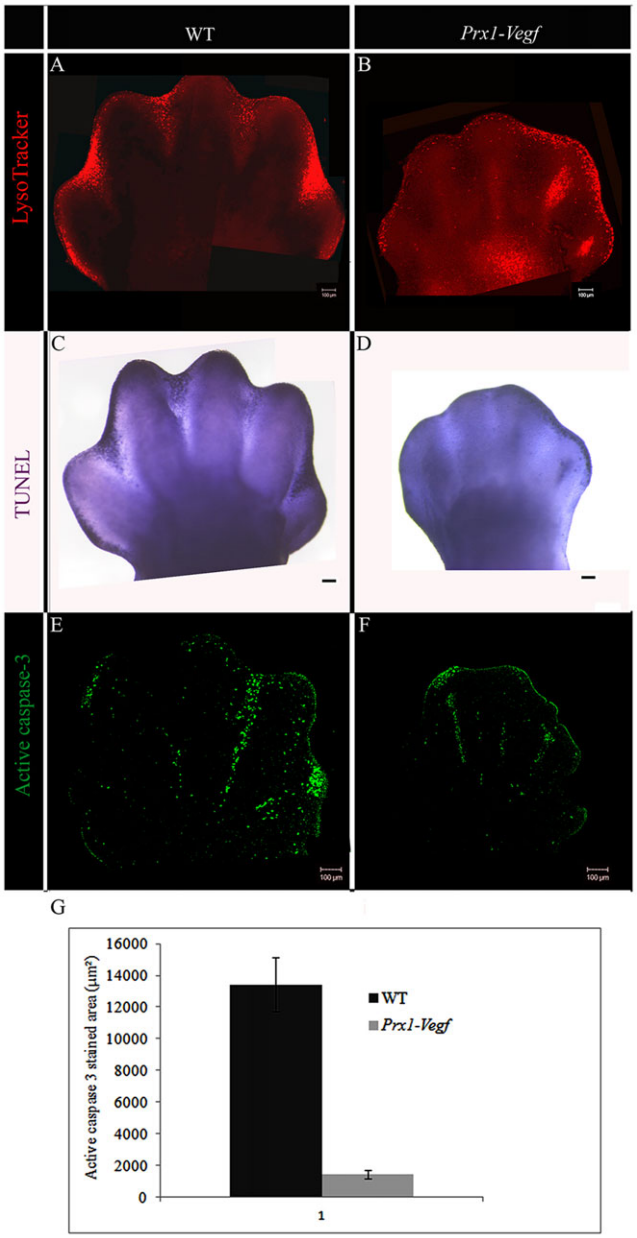

Fig. 3. A decrease in interdigital blood vessels leads to inhibition of PCD. (A,B) Whole-mount LysoTracker Red staining of E13.5 WT (A) and *Prx1-Vegf* (B) forelimbs. (C,D) Whole-mount TUNEL staining of E13.5 WT (C) and *Prx1-Vegf* (D) forelimbs. (E,F) Anti-active caspase-3 immunostaining of E13.5 WT (E) and *Prx1-Vegf* (F) forelimb cross-sections. Scale bars: 100 µm. (G) Comparison of anti-active caspase-3 staining between E13.5 WT and *Prx1-Vegf* forelimb cross-sections. n=3-7 different limbs; P<0.05; data represented as the mean±s.e.m.

markers for different patterning events during limb development. Analysis of the chondrogenic markers *Sox9* (Fig. 4A,B) and *Col2a1* (Fig. 4C,D) revealed a reduction in mesenchymal condensation and chondrocyte differentiation in the mutant limbs, resulting in severe skeletal abnormalities (Fig. 4E).

Finally, we analyzed the expression of genes that are known to regulate PCD in the limb. The aberrantly intact AER in the *Prx1-Vegf* limbs, as indicated by the expression of *Fgf8* (Fig. 4F,G) and *Bmp4* (Fig. 4H,I), raised the possibility that the genetic program that regulates PCD was affected in these mice. Further support for this assumption was the reduced expression of other components

Development (2015) 142, 672-680 doi:10.1242/dev.120279

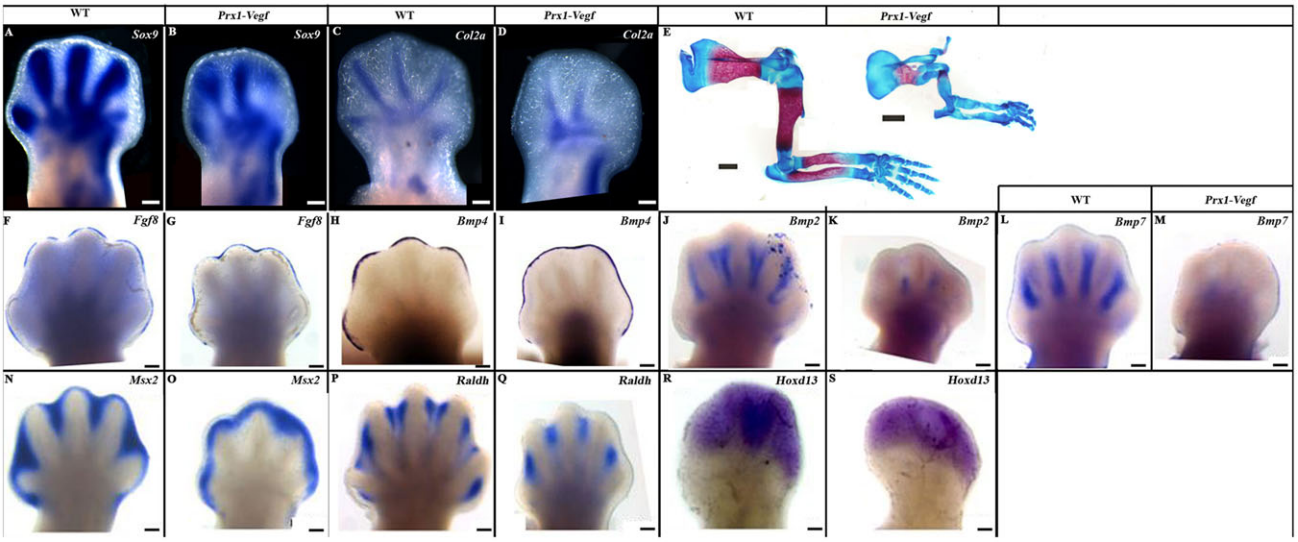

Fig. 4. Reduction in limb vasculature leads to a decrease in the expression of skeletogenesis and PCD gene markers. (A-D) Whole-mount *in situ* hybridization for *Sox9* (A,B) and *Col2a1* (C,D) in E12.5 WT and *Vegf-Prx1* forelimbs. (E) Alcian Blue (cartilage) and Alizarin Red (bone) stainings of E18.5 WT (left) and *Vegf-Prx1* forelimbs demonstrate impaired skeletal morphogenesis in the mutant. (F-I) *In situ* hybridization in WT and *Vegf-Prx1* whole-mount forelimbs for the expression of the AER markers *Fgf8* at E13.5 (F,G) and *Bmp4* at E12.5 (H,I). (J-S) Whole-mount *in situ* hybridization in E13.5 WT and *Vegf-Prx1* forelimbs for the expression of *Bmp2* (J,K), *Bmp7* (L,M), *Msx2* (N,O), *Raldh2* (P,Q) and *Hoxd13* (R,S). Scale bars: 200 µm in A-D,F-S; 1 mm in E.

of the PCD molecular mechanism, such as *Bmp2* (Fig. 4J,K), *Bmp7* (Fig. 4L,M) and *Msx2* (Fig. 4N,O), in *Prx1-Vegf* limbs relative to their expression in WT. Expression of *Raldh2* (Fig. 4P,Q) and *Hoxd13* (Fig. 4R,S) in the interdigital mesenchyme of *Prx1-Vegf* limbs ruled out the possibility that the reduction in the expression of PCD genes resulted from the loss of interdigital cell fate.

Taken together, these results suggest that a reduction in interdigital vessel number leads to inhibition of PCD. However, because of the developmental abnormalities observed in *Prx1-Vegf* limbs, a direct relationship between the reduced vasculature and the loss of PCD could not be established conclusively.

An increase in the number of interdigital blood vessels leads to expansion and elevation of PCD

The limitations of the *Vegf* loss-of-function model prompted us to consider a gain-of-function approach, i.e. to increase the number of blood vessels in the limb. For this, we overexpressed *Vegf* using a triple transgenic system, in which the expression of the reverse tetracycline transactivator (rtTA) and the tetracycline-responsive element (*tetO-Vegf165*) transgene system was induced by *Prx1-Cre* (Belteki et al., 2005; Benjamin and Keshet, 1997; Gossen et al., 1995). Induction of *Vegf* overexpression in E11.5 limbs resulted in a dramatic increase in vessel number, particularly in interdigital areas (Fig. 5A,B). Staining of E13.5 WT and *Vegf*-overexpressing autopods with LysoTracker (Fig. 5C,D), as well as terminal deoxynucleotidyl transferase dUTP nick end labeling (TUNEL) (Fig. 5E,F) and staining of active caspase-3 (Fig. 5G,H) revealed that increased vessel number led to an elevation in PCD and expansion of its domain. A comparison of stained cell numbers in WT and *Vegf*-overexpressing autopods (Fig. 5I) verified that result.

Although the transient nature of the gain-of-function model was expected to reduce indirect effects on interdigital PCD, we examined limb development upon *Vegf* overexpression. As evident from Alcian Blue staining and *Col2a1* expression, skeletogenesis in *Vegf*-overexpressing limbs was largely comparable to that of WT (Fig. 6A-B′). Similarly, expression of interdigital mesenchyme markers, such as *Raldh2* (Fig. 6C,C′), *Bmp2* (Fig. 6D,D′), *Bmp4* (Fig. 6E,E′) and *Msx* (Fig. 6F,F′), was comparable between *Vegf*-overexpressing and WT limbs. However, expression of the AER marker *Fgf8* was reduced in *Vegf*-overexpressing limbs relative to that of the control (Fig. 6G,G′), most likely indicating deterioration of the AER tissue. Together, these results strongly support a positive role for limb vasculature in the regulation of interdigital PCD.

Interdigital PCD is oxygen dependent

In order to uncover the mechanism underlying the positive role of vascular patterning in interdigital PCD, we first established an organ culture system that would serve to screen for different components of the mechanism. While using this system, we observed that upon incubation of the limb under ambient conditions (21% O_2), interdigital PCD increased in comparison to limbs that were examined before incubation (Fig. 7A,B). To further explore the possibility that interdigital PCD is oxygen dependent, we incubated E13.5 WT limbs under a gradient of oxygen levels and analyzed cell death. Analysis of LysoTracker (Fig. 7A-G), TUNEL (Fig. 7H-J,N) and active caspase-3 (Fig. 7K-N) staining revealed a clear correlation between oxygen levels and interdigital PCD, as limbs exposed to lower oxygen levels exhibited reduced signal. These results suggest that oxygen plays a key role in the mechanism that regulates interdigital PCD.

Interdigital oxidative stress is dependent on vascular patterning

Previous studies have implicated ROS in interdigital PCD, suggesting that interdigital cells are under oxidative stress. Our findings of the dependency of interdigital PCD on limb vasculature and oxygen level led us to hypothesize that the oxidative stress level in the interdigital zone is determined by changes in vascularization that, in turn, affect oxygen bioavailability. To test this hypothesis, we first studied the correlation between oxygen level and ROS production by incubating WT limbs in low (5%) or high (21%) oxygen levels. Similar to the PCD results, incubation in 21% oxygen resulted in higher ROS production relative to limbs

Development (2015) 142, 672-680 doi:10.1242/dev.120279

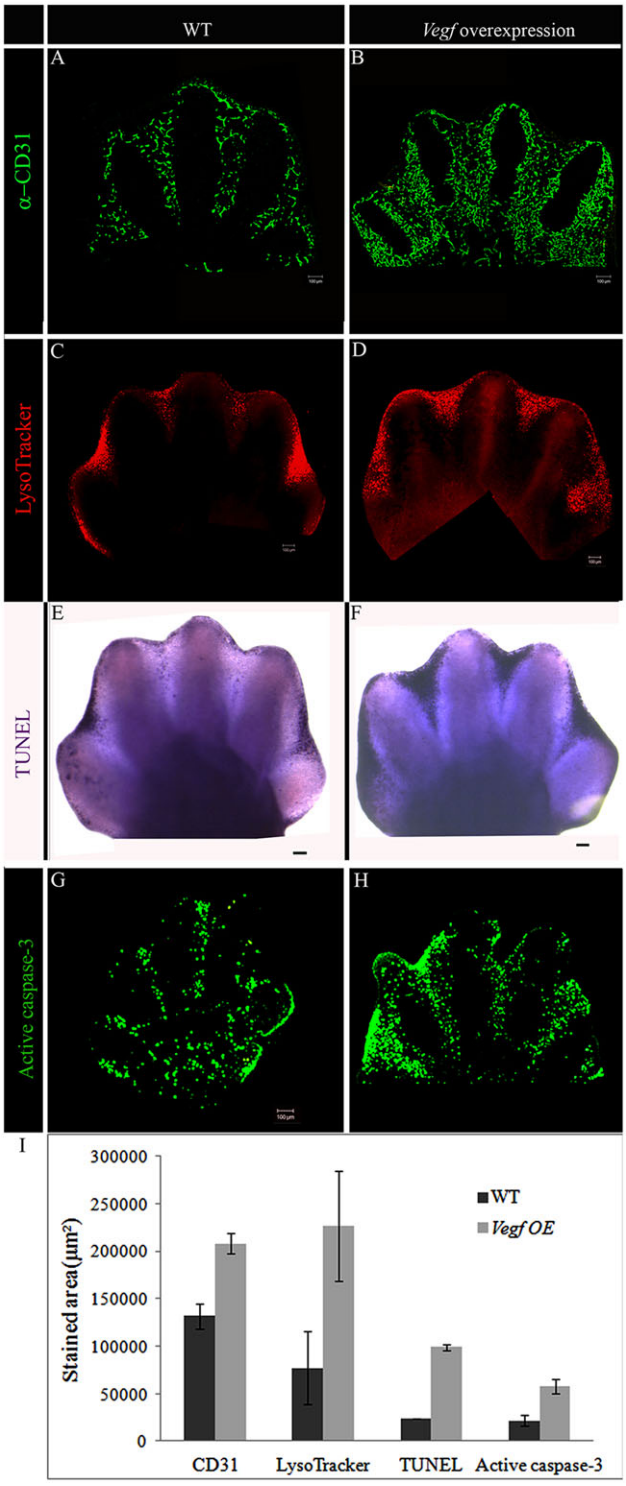

Fig. 5. Hypervascularization of limbs leads to an increase in PCD. (A,B) Whole-mount autopods of E13.5 WT and *Vegf*-overexpressing mice immunostained with anti-CD31 antibody (green) for vascular endothelial cells. (C,D) Whole-mount LysoTracker Red staining of E13.5 WT and *Vegf*-overexpressing autopods. (E,F) Whole-mount TUNEL staining of E13.5 WT and *Vegf*-overexpressing autopods. (G,H) Anti-active caspase-3 immunostaining of E13.5 WT and *Vegf*-overexpressing forelimb cross-sections. Scale bars: 100 µm. (I) Comparison of anti-CD31, LysoTracker Red, TUNEL and anti-active caspase-3 staining between E13.5 WT and *Vegf*-overexpressing (OE) forelimbs. n=3-7 different limbs; P<0.05 between WT and *Vegf* overexpression for all staining; data represent the mean±s.e.m.

incubated in 5% oxygen (Fig. 8A,B). Next, we examined ROS production in autopods of *Prx1-Vegf* and *Vegf*-overexpressing mice. Examination of E13.5 embryos showed a clear signal of ROS production primarily at the interdigital space of control limbs (Fig. 8C). In *Prx1-Vegf* limbs, the signal was dramatically reduced and could only be detected at the previously described apoptotic areas in the forming digits (Fig. 8D). By contrast, in limbs where *Vegf* was overexpressed, we observed an elevation in interdigital ROS production (Fig. 8E).

These results show high dependency of interdigital ROS production on blood vessel number and oxygen level. Moreover, they suggest the existence of a mechanism whereby a high level of blood vessels in the interdigital zone leads to an elevation in tissue oxygenation, which is needed for ROS production and, as a consequence, for PCD.

DISCUSSION

It is universally accepted that the vasculature is indispensable for embryonic development. In recent years, it has been firmly established that in addition to supplying oxygen and nutrients, the vasculature serves as a source of molecular signals that are essential for the development and morphogenesis of numerous organs (Crivellato et al., 2007; Nikolova and Lammert, 2003), including the heart, lungs, kidneys, pancreas and liver (Dor et al., 2001; Gao et al., 2005; Lammert et al., 2001; Matsumoto et al., 2001; Tirziu and Simons, 2009). During digit separation, interdigital AER and mesenchymal tissues undergo degeneration by PCD. Based on the role of the vasculature in organogenesis, previous studies in chick embryos examined the possible role of interdigital vessel regression in promoting this process. However, vessel regression was observed only at advanced stages of tissue degeneration (Fallon and Cameron, 1977; Hurle et al., 1985, 1986), leaving the role of vascular patterning in interdigital PCD unresolved. Our finding that the presence of vessels is necessary for interdigital PCD during mouse limb development suggests a new and previously unrecognized role of the vasculature in organ morphogenesis.

Limb morphogenesis is one of the most studied models for PCD. Extensive work has revealed that interdigital PCD is regulated by signals emanating from the interdigital mesenchyme and AER, forming a complex genetic network that controls this process (Hernández-Martínez and Covarrubias, 2011; Hurle et al., 1995; Montero and Hurlé, 2010). Yet, one question that has remained open regards the mechanisms that restrict PCD to interdigital areas. Our finding that the limb vasculature undergoes patterning just prior to the onset of PCD, resulting in rich interdigital vascular networks, suggests a possible role for vascular patterning in the regulation of PCD. This hypothesis is supported by our results showing a positive correlation between interdigital vessel number and PCD level, as well as dependency of PCD on oxygen level. Based on these findings, we suggest a mechanism whereby the spatial organization of the autopodial vasculature directs oxygen supply to interdigital cells but not to the forming digits, leading to an increase in ROS production and activation of PCD only in interdigital zones. This proposed mechanism adds a layer of regulation to PCD by restricting its domains to interdigital areas.

One result that appears not to be consistent with our model is the production of ROS by hypoxic condensation of *Prx1-Vegf* embryos. Under hypoxia, the concentration of O_2, a substrate for ROS production, is decreased. Indeed, the ‘paradox of increased reactive oxygen species during hypoxia’ is a well-known phenomenon, which was previously suggested to be a central component in the hypoxia-sensing mitochondrial mechanism (Guzy and Schumacker,

Development (2015) 142, 672-680 doi:10.1242/dev.120279

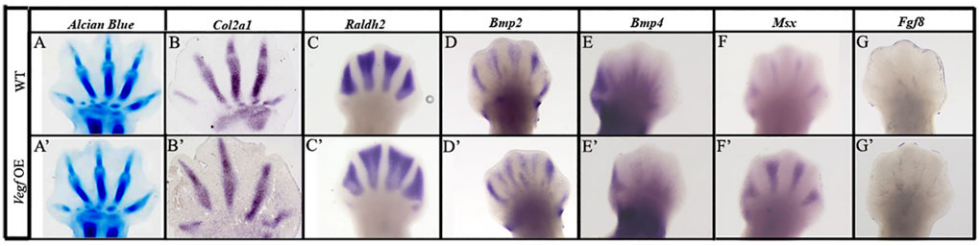

Fig. 6. Autopod development upon *Vegf* overexpression. Cartilage formation and expression of skeletogenic, interdigital and AER marker genes are shown in WT (upper panels) and *Vegf*-overexpressing (OE) forelimbs (lower panels) at E13.5. (A-B′) Chondrogenesis is detected by Alcian Blue staining (A,A′) and by *Col2a1* expression (B,B′). (C-F′) Expression of the interdigital markers *Raldh2* (C,C′), *Bmp2* (D,D′) *Bmp4* (E,E′) and *Msx* (F,F′). (G,G′) Expression of the AER marker *Fgf8*.

2006). Moreover, ROS production under hypoxia was demonstrated to activate hypoxia-inducible factor 1 (HIF-1) as part of the mechanism that allows cells to cope with these conditions (Chandel et al., 1998). Although the paradox and its significance are well known, the underlying mechanism is yet to be uncovered (Guzy and Schumacker, 2006).

Another interesting question relates to the integration between the genetic network that regulates interdigital PCD and the effect of the highly oxygenated environment formed by vascular patterning. Our analysis shows that although ROS production and PCD were markedly elevated in WT limbs incubated in high oxygen, they did not extend into the digits. This might suggest that the capacity of interdigital cells to produce ROS is determined by signaling pathways that have previously been shown to regulate interdigital PCD, such as the FGF, BMP and retinoic acid pathways (Dupé et al., 1999; Guha et al., 2002; Maatouk et al., 2009; Macias et al., 1997; Pajni-Underwood et al., 2007; Zou and Niswander, 1996). There are several possible mechanisms by which these factors can promote ROS production in interdigital mesenchymal cells. These include increasing the number of mitochondria, upregulation of proteins within the plasma membrane, such as NADPH oxidase and xanthine oxidase, and regulating lipid metabolism in the peroxisomes (Covarrubias et al., 2008). Interestingly, ROS are known to be signaling molecules; thus, ROS can serve as a reciprocal signal that drives the expression of key genes in the mechanism that regulates limb PCD. Alternatively, ROS signals might affect the composition of the extracellular matrix, which has also been implicated in PCD (Diaz-Mendoza et al., 2013).

Further support for the possible role of the vasculature and oxygen in interdigital PCD comes from various human pathologies, in which interruption in blood flow and/or oxygen supply are often associated with syndactyly and other skeletal deformities. Syndactyly associated with a decrease in embryonic oxygen supply is observed in congenital anemias, i.e. homozygous α-thalassemia, congenital dyserythropoietic anemia type I and Fanconi anemia (Abuelo et al., 1997; Adam et al., 2005; Brichard et al., 1994; Sadler and Rasmussen, 2010).

In this work, we suggest a new role for vascular patterning in controlling PCD during limb development. More broadly, our findings increase the scope of the involvement of blood vessels in development by showing that the vasculature promotes both tissue growth and death.

MATERIALS AND METHODS

Animals

The generation of *floxed-Vegf* (Gerber et al., 1999), *Prx1-Cre* (Logan et al., 2002), *rtTA* (Belteki et al., 2005) and *tetO-Vegf* (Benjamin and Keshet, 1997) mice has been described previously. To create *Prx1-Vegf* mice, males heterozygous for *Prx1-Cre* and for the *floxed-Vegf* allele were crossed with females homozygous for the *floxed-Vegf* allele and negative for *Prx1-Cre* mutation. As a control, embryos heterozygous for the *floxed-Vegf* allele with or without *Prx1-Cre* mutation were used.

To create *Vegf*-overexpressing mice, we used the reverse tetracycline transactivator (rtTA)/tetracycline-responsive element (tetO)-driven transgene system (Belteki et al., 2005; Gossen et al., 1995) with the *Prx1-Cre* mouse (Logan et al., 2002) as an inducer. Briefly, *tetO-Vegf* mice were crossed with *rtTA* mice. Female mice heterozygous for *rtTA* and *tetO-Vegf* (*rtTA-tetO-Vegf*) were crossed with males heterozygous for *Prx1-Cre*. To induce *Vegf* expression, doxycycline (3.33 µg/ml) was administered to pregnant females starting at E11.5. At E13.5, embryos heterozygous for *Prx1-Cre*, *rtTA* and *tetO-Vegf* (*Prx1-rtTA-tetO-Vegf*) were compared with embryos heterozygous for *rtTA* and *Prx1-Cre* alleles, as a control.

In all timed pregnancies, the day of the vaginal plug appearance was defined as E0.5. For harvesting of embryos, timed-pregnant female mice were sacrificed by CO_2 intoxication. The gravid uterus was dissected out and suspended in a bath of cold PBS, and the embryos were harvested after amnionectomy and removal of the placenta. Tail genomic DNA was used for genotyping. All experiments were performed with at least six different control and knockout forelimbs from three different litters.

Limb organ culture

Wild-type (WT) mouse forelimbs at E13.5 were cultured for 8 h at 37°C on 13 mm polycarbonate filters (Whatman) floating on BGJb medium (Gibco Invitrogen) containing 10% fetal bovine serum and 1% penicillin-streptomycin. To assess PCD sensitivity to oxygen levels, right-side forelimbs were incubated at different oxygen levels (5%, 10%, 12%, 15%, 21%) in a tri-gas incubator (Heraeus), in a humidified atmosphere balanced with N_2. Left-side forelimbs were used as control.

Whole-mount and section immunofluorescence

For whole-mount immunofluorescence, freshly dissected tissue was fixed overnight in 4% paraformaldehyde (PFA), transferred to PBS, then dehydrated to methanol as follows: 10 min in 25% methanol in PBS, 10 min in 50% methanol, 10 min in 75% methanol, then transferred to 100% methanol and stored at −20°C until use. Samples were rehydrated in PBS and incubated for 2 h in blocking solution (PBS containing 10% normal goat serum and 1% Triton X-100) to prevent nonspecific binding and then incubated overnight at 4°C with primary rat anti-PECAM antibody (CD31, BD Pharmingen; 1:25, diluted in blocking solution). Samples were washed in PBS containing 1% Triton X-100 at room temperature and then incubated overnight at 4°C with biotinylated anti-rat IgG secondary antibody (dilution 1:100; Vector Laboratories) and Cy2-conjugated streptavidin (1:100; Jackson ImmunoResearch) antibodies diluted in 1% BSA/PBS.

For frozen section immunofluorescence, embryo limbs were embedded in OCT (Tissue-Tek) after 2-6 h fixation in 4% PFA, and 12-µm-thick cryostat sections were created. Cryosections were postfixed for 30 min in 4% PFA and permeabilized with 0.2% Triton X-100 in PBS. In order to block nonspecific binding of immunoglobulin, sections were incubated with 7% goat serum in PBS. Following blocking, sections were incubated with primary antibody rat anti-CD31 (BD Pharmingen; 1:100) and secondary antibody Alexa Fluor 488-labeled goat anti-rat IgG.

Development (2015) 142, 672-680 doi:10.1242/dev.120279

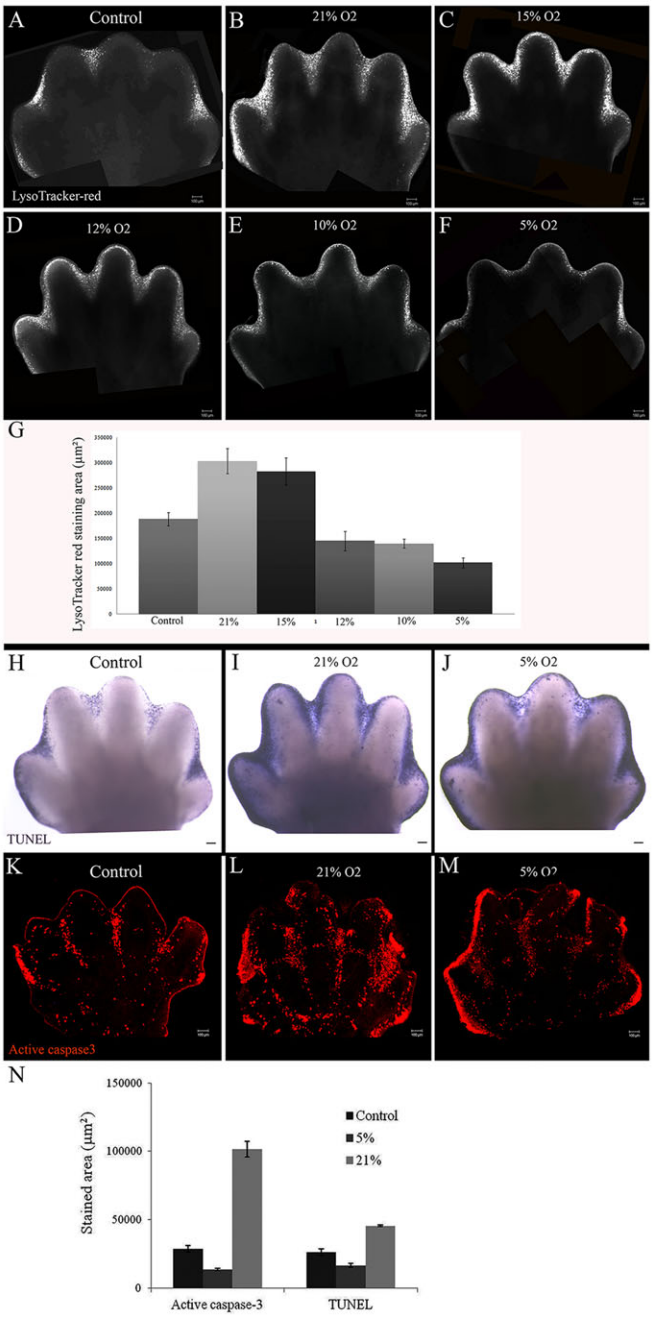

Fig. 7. Interdigital PCD is oxygen dependent. (A-F) Detection of PCD by whole-mount LysoTracker Red staining of E13.5 forelimbs before incubation (A) and after incubation in different oxygen levels (B-F). (G) Comparison of PCD quantified as mean LysoTracker Red-positive areas in control limbs (fresh) and in limbs incubated in 21%, 15%, 12%, 10% or 5% oxygen. *n*=3-7 different limbs; $P<0.05$ between control and 21% O_2 and between 21% and 5% O_2; data are represented as the mean±s.e.m. (H-J) Whole-mount TUNEL staining at E13.5 of fresh forelimbs (control; H) and of forelimbs incubated in 21% oxygen (I) or in 5% oxygen (J). (K-M) Whole-mount anti-active caspase-3 immunostaining at E13.5 of fresh forelimbs (control; K) and of forelimbs incubated in 21% oxygen (L) or in 5% oxygen (M). Scale bars: 100 µm. (N) Comparison of TUNEL and anti-active caspase-3 stained areas in E13.5 control limbs and limbs incubated in 21% O_2 and 5% O_2. *n*=3-7 different limbs; $P<0.05$ between 5% and 21% O_2 for all staining; data are represented as the mean±s.e.m.

For paraffin section immunofluorescence, embryo limbs were fixed overnight in 4% PFA at 4°C, embedded in paraffin and sectioned at a thickness of 7 µm. Antigen was retrieved in 10 mM citrate buffer (pH 6.0) using a microwave. In order to block nonspecific binding of immunoglobulin, sections were incubated with 7% goat serum. Then, sections were incubated overnight at 4°C with rabbit anti-activated caspase-3 (Asp 175) antibody (1:50; Cell Signaling Technology). Sections were washed in 0.1% Tween 20 in PBS and incubated with Cy2-conjugated or Cy3-conjugated secondary fluorescent antibodies (1:100; Jackson Laboratories). Frozen and paraffin sections were washed and mounted on glass slides. Whole-mounts and sections were examined by microscopy (see below).

Image processing

Multiple panels in Figs 1, 3, 5, 7 and 8 were generated from composite images, because the samples were too large to fit in a single field of view at high resolution. Images were then stitched together in Adobe Photoshop.

Cell death detection

For LysoTracker staining, freshly dissected whole-mount forelimbs were incubated with LysoTracker Red (Molecular Probes; 2 µg/ml in PBS) at 37°C for 30 min; aluminium foil was used to avoid exposure to light. Confocal imaging is described below. For the TUNEL assay, freshly dissected whole-mount forelimbs were fixed overnight in 4% PFA, dehydrated to methanol:H_2O_2 (5:1) and incubated with proteinase K (5 µg/ml). Tissues were fixed in 4% PFA, 0.1% glutaraldehyde, 0.1% sodium borohydride solution for 20 min and then stained using the *In Situ* Cell Death Detection Kit (Roche Diagnostics), according to the manufacturer's instructions.

Skeletal preparations, *in situ* hybridization and histology

Cartilage and bones in whole mouse embryos were visualized after staining with Alcian Blue and Alizarin Red S (Sigma) and clarification of soft tissue with potassium hydroxide (McLeod, 1980). For histology and *in situ* hybridization, embryos were fixed overnight in 4% PFA, dehydrated to 100% ethanol, embedded in paraffin and sectioned at a thickness of 7 µm. For *in situ* hybridization, embryos were fixed overnight in 4% PFA. Section and whole-mount *in situ* hybridizations were performed as described previously (Riddle et al., 1993). All probes are available upon request. Hematoxylin and Eosin (H&E) staining was performed following standard protocols.

ROS detection and microscopy

To determine ROS levels, whole-mount forelimbs were incubated in 10 µM dihydroethidium (DHE) in PBS (pH 6.5) at 37°C for 30 min and examined by microscopy. Confocal imaging was performed using an LSM510 laser-scanning confocal microscope (Carl Zeiss). *z*-stacks were acquired at 2.5 µm increments and images were converted to grayscale and processed offline with ImageJ software (National Institutes of Health).

Quantification of staining and statistical analysis

Quantification of CD31-stained vessels and of LysoTracker Red, TUNEL and active caspase-3 staining was performed on transverse and longitudinal sections using ImageJ. Individual images were converted to grayscale by RGB splitting, and the green channel was used for CD31 and active caspase-3, and the red channel was used for LysoTracker Red and TUNEL. Images were thresholded to separate positively stained areas, which were then calculated. Data are presented as the mean±s.e.m. Comparisons between WT and mutant embryos were carried out using Student's *t*-test, and statistical significance was defined as $P \leq 0.05$.

Acknowledgements

We thank N. Konstantin for expert editorial assistance. Special thanks to all members of the E.Z. laboratory for their advice and suggestions.

Competing interests

The authors declare no competing or financial interests.

Author contributions

I.E.-O. conducted experiments and data analyses and wrote the manuscript. S.K. conducted experiments and data analyses. N.F. provided the *Vegf*-, *Flt1*- and

Development (2015) 142, 672-680 doi:10.1242/dev.120279

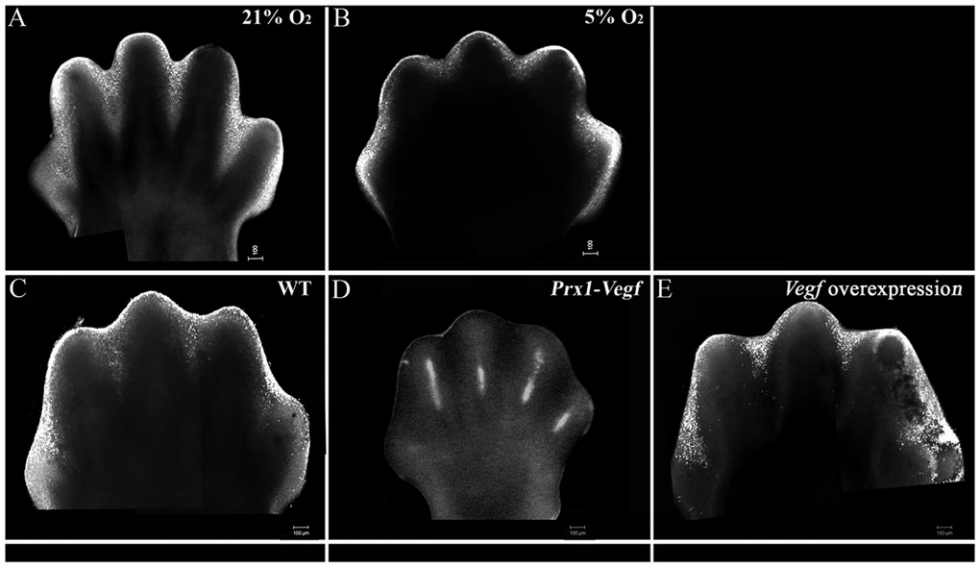

Fig. 8. Interdigital ROS production is dependent on oxygen level and vascular patterning. Detection of ROS production by whole-mount staining of forelimbs with DHE, as a marker for superoxide. (A,B) E13.5 WT forelimbs incubated in high (21%; A) or low (5%; B) oxygen levels. (C-E) Forelimbs from WT (C), *Prx1-Vegf* (D) and *Vegf*-overexpressing (E) embryos at E13.5. Scale bars: 100 µm.

Flk1-floxed mice. A.M.E. provided advice on human skeletal deformities related to vascular abnormalities. E.Z. conducted data analyses, wrote the manuscript and supervised the project.

Funding

This work was supported by grants from the United States-Israel Binational Science Foundation (BSF) [grant number 2011122]; the European Research Council (ERC) [grant number 310098]; and the Minerva Foundation [grant number 711428], all to E.Z.

References

Abuelo, D. N., Forman, E. N. and Rubin, L. P. (1997). Limb defects and congenital anomalies of the genitalia in an infant with homozygous alpha-thalassemia. *Am. J. Med. Genet.* **68**, 158-161.

Adam, M. P., Chueh, J., El-Sayed, Y. Y., Stenzel, A., Vogel, H., Weaver, D. D. and Hoyme, H. E. (2005). Vascular-type disruptive defects in fetuses with homozygous alpha-thalassemia: report of two cases and review of the literature. *Prenat. Diagn.* **25**, 1088-1096.

Belteki, G., Haigh, J., Kabacs, N., Haigh, K., Sison, K., Costantini, F., Whitsett, J., Quaggin, S. E. and Nagy, A. (2005). Conditional and inducible transgene expression in mice through the combinatorial use of Cre-mediated recombination and tetracycline induction. *Nucleic Acids Res.* **33**, e51.

Benjamin, L. E. and Keshet, E. (1997). Conditional switching of vascular endothelial growth factor (VEGF) expression in tumors: induction of endothelial cell shedding and regression of hemangioblastoma-like vessels by VEGF withdrawal. *Proc. Natl. Acad. Sci. USA* **94**, 8761-8766.

Bokov, A., Chaudhuri, A. and Richardson, A. (2004). The role of oxidative damage and stress in aging. *Mech. Ageing Dev.* **125**, 811-826.

Brichard, B., Vermylen, C., Scheiff, J. M., Michaux, J. L., Ninane, J. and Cornu, G. (1994). Two cases of congenital dyserythropoietic anaemia type I associated with unusual skeletal abnormalities of the limbs. *Br. J. Haematol.* **86**, 201-202.

Carmeliet, P. (2005). Angiogenesis in life, disease and medicine. *Nature* **438**, 932-936.

Chandel, N. S., Maltepe, E., Goldwasser, E., Mathieu, C. E., Simon, M. C. and Schumacker, P. T. (1998). Mitochondrial reactive oxygen species trigger hypoxia-induced transcription. *Proc. Natl. Acad. Sci. USA* **95**, 11715-11720.

Cleaver, O. and Melton, D. A. (2003). Endothelial signaling during development. *Nat. Med.* **9**, 661-668.

Coffin, J. D. and Poole, T. J. (1988). Embryonic vascular development: immunohistochemical identification of the origin and subsequent morphogenesis of the major vessel primordia in quail embryos. *Development* **102**, 735-748.

Cooper, K. L., Hu, J. K.-H., ten Berge, D., Fernandez-Teran, M., Ros, M. A. and Tabin, C. J. (2011). Initiation of proximal-distal patterning in the vertebrate limb by signals and growth. *Science* **332**, 1083-1086.

Coultas, L., Chawengsaksophak, K. and Rossant, J. (2005). Endothelial cells and VEGF in vascular development. *Nature* **438**, 937-945.

Covarrubias, L., Hernández-García, D., Schnabel, D., Salas-Vidal, E. and Castro-Obregón, S. (2008). Function of reactive oxygen species during animal development: passive or active? *Dev. Biol.* **320**, 1-11.

Crivellato, E., Nico, B. and Ribatti, D. (2007). Contribution of endothelial cells to organogenesis: a modern reappraisal of an old Aristotelian concept. *J. Anat.* **211**, 415-427.

Díaz-Mendoza, M. J., Lorda-Diez, C. I., Montero, J. A., García-Porrero, J. A. and Hurlé, J. M. (2013). Interdigital cell death in the embryonic limb is associated with depletion of Reelin in the extracellular matrix. *Cell Death Dis.* **4**, pe800.

Dor, Y., Camenisch, T. D., Itin, A., Fishman, G. I., McDonald, J. A., Carmeliet, P. and Keshet, E. (2001). A novel role for VEGF in endocardial cushion formation and its potential contribution to congenital heart defects. *Development* **128**, 1531-1538.

Drake, C. J., Hungerford, J. E. and Little, C. D. (1998). Morphogenesis of the first blood vessels. *Ann. N. Y. Acad. Sci.* **857**, 155-179.

Dunwoodie, S. L. (2009). The role of hypoxia in development of the Mammalian embryo. *Dev. Cell* **17**, 755-773.

Dupé, V., Ghyselinck, N. B., Thomazy, V., Nagy, L., Davies, P. J. A., Chambon, P. and Mark, M. (1999). Essential roles of retinoic acid signaling in interdigital apoptosis and control of BMP-7 expression in mouse autopods. *Dev. Biol.* **208**, 30-43.

Eshkar-Oren, I., Viukov, S. V., Salameh, S., Krief, S., Oh, C.-d., Akiyama, H., Gerber, H.-P., Ferrara, N. and Zelzer, E. (2009). The forming limb skeleton serves as a signaling center for limb vasculature patterning via regulation of Vegf. *Development* **136**, 1263-1272.

Fallon, J. F. and Cameron, J. (1977). Interdigital cell death during limb development of the turtle and lizard with an interpretation of evolutionary significance. *J. Embryol. Exp. Morphol.* **40**, 285-289.

Feinberg, R. N., Latker, C. H. and Beebe, D. C. (1986). Localized vascular regression during limb morphogenesis in the chicken embryo. I. Spatial and temporal changes in the vascular pattern. *Anat. Rec.* **214**, 405-409.

Fernandez-Teran, M. and Ros, M. A. (2008). The apical ectodermal ridge: morphological aspects and signaling pathways. *Int. J. Dev. Biol.* **52**, 857-871.

Fernández-Terán, M. A., Hinchliffe, J. R. and Ros, M. A. (2006). Birth and death of cells in limb development: a mapping study. *Dev. Dyn.* **235**, 2521-2537.

Ferrara, N., Carver-Moore, K., Chen, H., Dowd, M., Lu, L., O'Shea, K. S., Powell-Braxton, L., Hillan, K. J. and Moore, M. W. (1996). Heterozygous embryonic lethality induced by targeted inactivation of the VEGF gene. *Nature* **380**, 439-442.

Folkman, J. (2003). Fundamental concepts of the angiogenic process. *Curr. Mol. Med.* **3**, 643-651.

Gao, X., Chen, X., Taglienti, M., Rumballe, B., Little, M. H. and Kreidberg, J. A. (2005). Angioblast-mesenchyme induction of early kidney development is mediated by Wt1 and Vegfa. *Development* **132**, 5437-5449.

Gerber, H. P., Hillan, K. J., Ryan, A. M., Kowalski, J., Keller, G. A., Rangell, L., Wright, B. D., Radtke, F., Aguet, M. and Ferrara, N. (1999). VEGF is required for growth and survival in neonatal mice. *Development* **126**, 1149-1159.

Gossen, M., Freundlieb, S., Bender, G., Muller, G., Hillen, W. and Bujard, H. (1995). Transcriptional activation by tetracyclines in mammalian cells. *Science* **268**, 1766-1769.

Guha, U., Gomes, W. A., Kobayashi, T., Pestell, R. G. and Kessler, J. A. (2002). In vivo evidence that BMP signaling is necessary for apoptosis in the mouse limb. *Dev. Biol.* **249**, 108-120.

Guzy, R. D. and Schumacker, P. T. (2006). Oxygen sensing by mitochondria at complex III: the paradox of increased reactive oxygen species during hypoxia. *Exp. Physiol.* **91**, 807-819.

Hall, B. K. and Miyake, T. (1992). The membranous skeleton: the role of cell condensations in vertebrate skeletogenesis. *Anat. Embryol. (Berl.)* **186**, 107-124.

Hernández-Martíinez, R. and Covarrubias, L. (2011). Interdigital cell death function and regulation: new insights on an old programmed cell death model. *Dev. Growth Differ.* **53**, 245-258.

Hernandez-Martinez, R., Castro-Obregon, S. and Covarrubias, L. (2009). Progressive interdigital cell death: regulation by the antagonistic interaction between fibroblast growth factor 8 and retinoic acid. *Development* **136**, 3669-3678.
Hurle, J. M., Colvee, E. and Fernandez-Teran, M. A. (1985). Vascular regression during the formation of the free digits in the avian limb bud: a comparative study in chick and duck embryos. *J. Embryol. Exp. Morphol.* **85**, 239-250.
Hurle, J. M., Fernandez-Teran, M. A. and Colvee, E. (1986). Regression of the interdigital tissue during the formation of the digits. *Acta Histochem. Suppl.* **32**, 165-169.
Hurle, J. M., Ros, M. A., Garcia-Martinez, V., Macias, D. and Ganan, Y. (1995). Cell death in the embryonic developing limb. *Scanning Microsc.* **9**, 519-533; discussion 533-514.
Johnson, R. L. and Tabin, C. J. (1997). Molecular models for vertebrate limb development. *Cell* **90**, 979-990.
Lallemand, Y., Nicola, M.-A., Ramos, C., Bach, A., Cloment, C. S. and Robert, B. (2005). Analysis of Msx1; Msx2 double mutants reveals multiple roles for Msx genes in limb development. *Development* **132**, 3003-3014.
Lammert, E., Cleaver, O. and Melton, D. (2001). Induction of pancreatic differentiation by signals from blood vessels. *Science* **294**, 564-567.
Logan, M., Martin, J. F., Nagy, A., Lobe, C., Olson, E. N. and Tabin, C. J. (2002). Expression of Cre Recombinase in the developing mouse limb bud driven by a Prxl enhancer. *Genesis* **33**, 77-80.
Maatouk, D. M., Choi, K.-S., Bouldin, C. M. and Harfe, B. D. (2009). In the limb AER Bmp2 and Bmp4 are required for dorsal-ventral patterning and interdigital cell death but not limb outgrowth. *Dev. Biol.* **327**, 516-523.
Macias, D., Ganan, Y., Sampath, T. K., Piedra, M. E., Ros, M. A. and Hurle, J. M. (1997). Role of BMP-2 and OP-1 (BMP-7) in programmed cell death and skeletogenesis during chick limb development. *Development* **124**, 1109-1117.
Matsumoto, K., Yoshitomi, H., Rossant, J. and Zaret, K. S. (2001). Liver organogenesis promoted by endothelial cells prior to vascular function. *Science* **294**, 559-563.
McLeod, M. J. (1980). Differential staining of cartilage and bone in whole mouse fetuses by alcian blue and alizarin red S. *Teratology* **22**, 299-301.
Montero, J. A. and Hurlé, J. M. (2010). Sculpturing digit shape by cell death. *Apoptosis* **15**, 365-375.
Montero, J. A., Ganan, Y., Macias, D., Rodriguez-Leon, J., Sanz-Ezquerro, J. J., Merino, R., Chimal-Monroy, J., Nieto, M. A. and Hurle, J. M. (2001). Role of FGFs in the control of programmed cell death during limb development. *Development* **128**, 2075-2084.
Nikolova, G. and Lammert, E. (2003). Interdependent development of blood vessels and organs. *Cell Tissue Res.* **314**, 33-42.
Pajni-Underwood, S., Wilson, C. P., Elder, C., Mishina, Y. and Lewandoski, M. (2007). BMP signals control limb bud interdigital programmed cell death by regulating FGF signaling. *Development* **134**, 2359-2368.
Riddle, R. D., Johnson, R. L., Laufer, E. and Tabin, C. (1993). Sonic hedgehog mediates the polarizing activity of the ZPA. *Cell* **75**, 1401-1416.
Risau, W. and Flamme, I. (1995). Vasculogenesis. *Annu. Rev. Cell Dev. Biol.* **11**, 73-91.
Rodriguez-Leon, J., Merino, R., Macias, D., Gañan, Y., Santesteban, E. and Hurle, J. M. (1999). Retinoic acid regulates programmed cell death through BMP signalling. *Nat. Cell Biol.* **1**, 125-126.
Sabin, R. (1920). Studies on the origin of blood vessels and of red blood corpuscles as seen in the living blastoderm of chick during the second day of incubation. *Contrib. Embryol. Carnegie Inst.* **9**, 215-262.
Sadler, T. W. and Rasmussen, S. A. (2010). Examining the evidence for vascular pathogenesis of selected birth defects. *Am. J. Med. Genet. A* **152A**, 2426-2436.
Salas-Vidal, E., Lomeli, H., Castro-Obregón, S., Cuervo, R., Escalante-Alcalde, D. and Covarrubias, L. (1998). Reactive oxygen species participate in the control of mouse embryonic cell death. *Exp. Cell Res.* **238**, 136-147.
Salas-Vidal, E., Valencia, C. and Covarrubias, L. (2001). Differential tissue growth and patterns of cell death in mouse limb autopod morphogenesis. *Dev. Dyn.* **220**, 295-306.
Sato, T. and Loughna, S. (2002). Vasculogenesis and angiogenesis. In *Mouse Development*, pp. 211-230. Academic Press.
Schnabel, D., Salas-Vidal, E., Narváez, V., Sánchez-Carbente, M. d. R., Hernández-García, D., Cuervo, R. and Covarrubias, L. (2006). Expression and regulation of antioxidant enzymes in the developing limb support a function of ROS in interdigital cell death. *Dev. Biol.* **291**, 291-299.
Seichert, V. and Rychter, Z. (1972). Vascularization of the developing anterior limb of the chick embryo. 3. Developmental changes in the perimetacarpal capillary network. *Folia Morphol. (Praha)* **20**, 397-405.
Tirziu, D. and Simons, M. (2009). Endothelium as master regulator of organ development and growth. *Vascul. Pharmacol.* **50**, 1-7.
Zeller, R., López-Ríos, J. and Zuniga, A. (2009). Vertebrate limb bud development: moving towards integrative analysis of organogenesis. *Nat. Rev. Genet.* **10**, 845-858.
Zou, H. and Niswander, L. (1996). Requirement for BMP signaling in interdigital apoptosis and scale formation. *Science* **272**, 738-741.
Zuzarte-Luis, V. and Hurle, J. M. (2002). Programmed cell death in the developing limb. *Int. J. Dev. Biol.* **46**, 871-876.